Experimental characterization of dislocations in deformation induced planar boundaries of rolled aluminium

Hong, Chuanshi; Huang, Xiaoxu; Winther, Grethe

Published in:
Risoe International Symposium on Materials Science. Proceedings

Publication date:
2012

Document Version
Publisher's PDF, also known as Version of record

Proceedings of the 33rd
Risø International Symposium on Materials Science:
Nanometals – Status and Perspective
Editors: S. Fæster, N. Hansen, X. Huang,
D. Juul Jensen and B. Ralph
Department of Wind Energy
Technical University of Denmark, 2012

EXPERIMENTAL CHARACTERIZATION OF DISLOCATIONS IN DEFORMATION INDUCED PLANAR BOUNDARIES OF ROLLED ALUMINIUM

C.S. Hong*, X. Huang* and G. Winther**

*Danish-Chinese Center for Nanometals, Materials Science and Advanced Characterization Section, Department of Wind Energy, Technical University of Denmark, DK-4000 Roskilde, Denmark
**Department of Mechanical Engineering, Technical University of Denmark, DK-2800 Kgs. Lyngby, Denmark

ABSTRACT

Dislocations in 2 geometrically necessary boundaries in a grain near the 45°-ND rotated cube orientation in 10% rolled 99.996% pure Al were investigated by detailed transmission electron microscopy. In these two boundaries dislocations with all six Burgers vectors of the ½<110> type expected for fcc crystals were observed but dislocations from the four most active slip systems dominated. The dislocations with Burgers vectors not corresponding to one of the expected active slip systems are primarily interpreted as being the result of dislocation reactions in the boundary. Two main types of dislocation networks in the boundaries were observed: (1) 3 sets of dislocations in a hexagonal network all having Burgers vectors in the slip plane with which the boundary aligned. Two of these come from the active slip systems, the third is attributed to dislocation reactions. (2) 4 sets of dislocations of which one was a Lomer lock formed by two other dislocation sets. This type of boundary contains dislocations coming from both of the slip planes expected active.

1. INTRODUCTION

During plastic deformation of metals the gliding dislocations interact to give work-hardening and also to form dislocation boundaries, which develop into a regular deformation microstructure within each grain. Morphologically, dislocation boundaries fall in two main categories, one being extended planar boundaries with a specific crystallographic alignment and the other being a three-dimensional arrangement of shorter boundaries forming a fairly equiaxed cell structure (Bay, Hansen, Hughes and

Kuhlmann-Wilsdorf 1992; Wert, Huang, Winther, Pantleon and Poulsen 2007). The extended planar boundaries are termed Geometrically Necessary Boundaries (GNBs) and the randomly oriented boundaries in the equiaxed cell structures are termed Incidental Dislocation Boundaries (IDBs). Most often the microstructure in a grain consists of one or two sets of parallel GNBs, in between which IDBs forming a cell structure are found. In combination the GNBs and IDBs form a cell block structure.

The morphology as well as the crystallographic alignment of the dislocation boundaries depend strongly on the crystallographic orientation of the grain (Huang and Winther 2007; Lin, Godfrey and Winther 2009). Recent research has furthermore shown that the type of dislocation boundaries formed can be predicted based on the slip systems expected to be active (Winther and Huang 2007; Winther 2008). The strong relationship between the type of boundaries and the active slip systems suggests that the dislocations in the boundaries are those coming from the active slip systems and that they interact in a systematic manner to form boundaries with similar characteristics, resulting in the regular microstructure within each grain. Recently the dislocation content was characterised by transmission electron microscopy (TEM) in many similarly oriented IDBs in an equiaxed cell structure found in rolled grains of near cube orientation (Wei, Godfrey, Liu, Liu, Huang, Hansen and Winther 2011). All the investigated boundaries contained dislocations which had Burgers vectors corresponding to the active slip directions.

The dislocation content in GNBs in the form of Burgers vectors and line directions has so far only been characterised for a few special cases, namely GNBs aligned with a slip plane (Hughes, Khan, Godfrey and Zbib 2001; McCabe, Misra and Mitchell 2004). Dislocations forming the boundary can give important information on how the GNBs form and evolve during plastic deformation, and also how the GNB structure can affect the flow stress and flow stress anisotropy of plastically deformed samples (Hansen and Huang 1998; Winther 2005). The current paper presents detailed experimental characterisation of the dislocations within 2 slip-plane-aligned GNBs coming from a grain of near 45°-ND rotated cube orientation in rolled pure aluminium. These GNBs are aligned with the two active slip planes as well-established for single crystals, see e.g. (Li, Godfrey and Liu 2004), and as illustrated in Fig. 1.

2. EXPERIMENTAL

A high-purity Al (99.996%) sheet of 2 mm thickness was annealed at 300 °C for 2 h, resulting in an average grain size of 70 μm and a strong cube texture. Rectangular samples of dimensions 2×10×40 mm^3 were cut out to produce smaller sheets rotated 45° around the sheet normal. In these smaller sheets grains with an orientation deviating less than 15° from the ideal 45°-ND rotated cube orientation consume a volume fraction of larger than 85%. The sheets were rolled in a single pass by 10% in thickness reduction at room temperature. The amount of deformation is sufficient for typical GNBs to form while it keeps the dislocation density at a relatively low level to facilitate TEM observations. Some observations of the overall deformed structures were carried out on specimens prepared from the longitudinal section (containing the rolling direction, RD, and normal direction, ND) by electron channelling contrast (ECC) on a Zeiss Supra 35 scanning electron microscope (SEM). Detailed observations of the dislocation boundaries were then carried out by TEM on a JEOL 2000FX electron microscope, which was operated at a low voltage of 120 kV to minimize damage induced by electron irradiation.

The TEM foils were prepared from the rolling-plane section. For a grain with ideal 45°-ND rotated

cube orientation, the two possible sets of GNBs are expected to incline at 55° to the foil plane and both contain the transverse direction (TD) of rolling, as in Fig. 1a. These foils were mounted onto the TEM holder with TD parallel to the holder axis-x, so that when the foil is tilted around the holder axis-x in the positive and negative directions, both an edge-on view and a nearly lie-flat view of the GNBs are possible for both sets of GNBs.

To examine the dislocation configurations and contributing Burgers vectors, **b**, in the GNBs, two-beam diffraction contrast experiments were carried out using different diffraction vectors, **g**. The weak-beam technique was employed using a (**g**/3**g**) diffraction condition to obtain sharp images. For each analyzed GNB, the dislocation configurations were represented by schematic lines extracted from the corresponding two-beam diffraction contrast images. A color scheme as shown in Fig. 1b was applied for the schematic dislocation lines to indicate their **b**. For convenience, hereafter the Burgers vectors $\pm\frac{1}{2}[10\bar{1}]$, $\pm\frac{1}{2}[01\bar{1}]$, $\pm\frac{1}{2}[1\bar{1}0]$, $\pm\frac{1}{2}[101]$, $\pm\frac{1}{2}[011]$ and $\pm\frac{1}{2}[110]$ are referred to as **b1**, **b2**,… and **b6**, respectively. Note that **b1** and **b2** on (111), as well as **b4** and **b5** on $(11\bar{1})$, are two sets of coplanar slip systems predicted active; whereas **b3** and **b6** are predicted inactive.

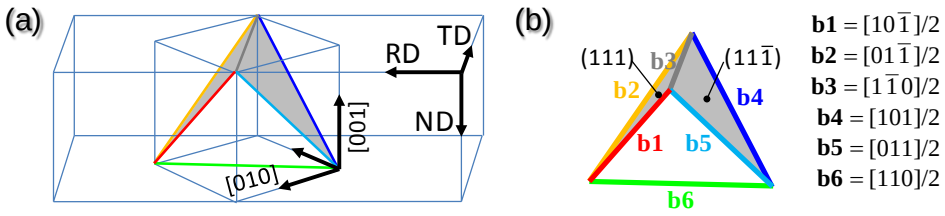

Fig. 1. (a) Rolling geometry. RD, TD and ND refer to the rolling, transverse and normal directions, respectively. Coplanar slip planes predicted active are indicated by gray. (b) Colour scheme for tracing of dislocations according to Burgers vectors.

3. RESULTS

An example ECC micrograph of the deformed microstructures from the longitudinal section is shown in Fig. 2a. Due to the sensitivity of ECC to grain orientation, only a portion of grains have their inner microstructures revealed. For all these grains, pronounced GNBs are observed. In a majority of grains, there are two sets of crisscrossing GNBs; whereas in a minority of grains only one pronounced set of GNBs is observed. For the grains with two sets of GNBs, in most cases one set is prominent and apparently more pronounced than the other; only in a few cases the two sets of GNBs appear equally developed. In the rolling-plane section examined by TEM (Fig. 2b), extended GNBs, which normally have a length of several to tens of micrometers and are considerably straight, are found in all the grains observed. In general, these boundaries are aligned with TD, which agrees well the expectation that for grains with an ideal rotated-cube orientation, the traces of two sets of GNBs should coincide in the rolling plane, and should be parallel to TD.

Two boundaries, hereafter termed GNB-I and GNB-II were chosen from a grain in the rolling-plane section for detailed TEM investigation. The grain has the orientation of ND/RD=(-0.057 0.045 -0.997)/[0.647 0.763 -0.003], 6.2° away from the ideal orientation. As will be shown in Section 3.1, GNB-I is aligned near (111) and GNB-II is near $(11\bar{1})$.

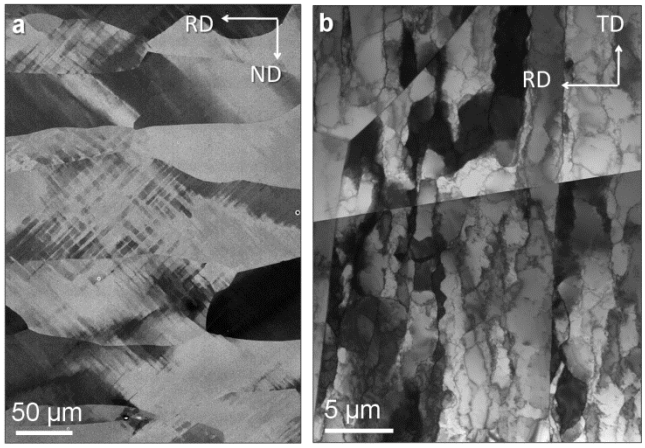

Fig. 2. (a) ECC observation of the deformed microstructure from the longitudinal section. (b) TEM observation at low magnification of the deformed microstructure from the rolling-plane section.

3.1 Examination of 3-dimensional dislocation arrangements and determination of boundary planes. The 3-dimensional dislocation arrangements for either of the two GNBs were examined by taking serial 2-dimensional projection images at incremental tilts. The serial tilting was done around TD, which is close to the GNB traces, with an incremental tilt step of 2-10°. Figure 3 gives an image series of GNB-I at several representative tilting positions. It is found that most of the dislocations are indeed well organized into a reasonably flat, 2-dimensional network, forming a boundary. As the tilting angle varies from -42° towards 40.3°, the projected width of the majority part of the dislocation network first continuously decreases from Fig. 3a to b, and afterwards increases from Fig. 3b to f. In Fig. 3b, the upper and lower parts of the dislocation network appear most close to being edge-on (perpendicular to the imaging plane). Besides the boundary dislocations, there are a few dislocations which do not lie in the boundary. For example, the dislocations indicated by white arrows are obviously out of the boundary in Fig. 3b, but they overlap with the boundary dislocations in Fig. 3f where the boundary lies flat to the viewing plane. These dislocations are not analyzed as focus is on the dislocations organized in boundaries.

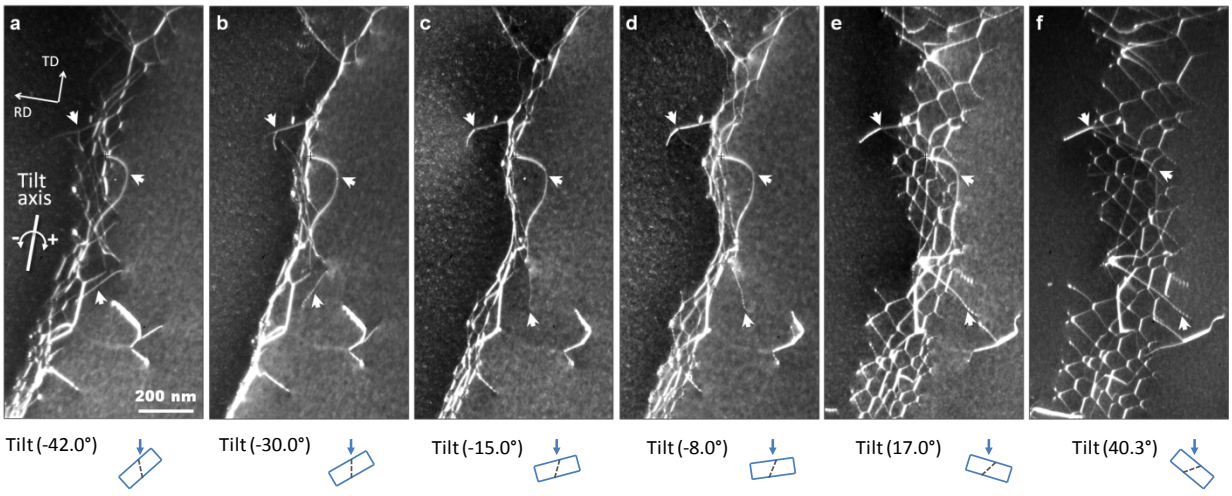

Fig. 3. Incremental tilting around TD to examine 3-dimensional arrangement of dislocations in GNB-I. Weak-beam images using **g**=[2 $\bar{2}$ 0]. Inclinations of foil and the GNB relative to the beam direction at each tilt position are illustrated under the corresponding image, where the blue arrow indicates the beam direction, the rectangular frame represents the foil, and the gray line represents the GNB. White arrows in each image marked the positions at different tilts of dislocations that do not lie in the boundary.

The precise alignments of the two GNBs were then determined using the edge-on technique (Huang and Liu 1998). To be brief, the alignment of a given GNB is determined by tilting the TEM foil to a position where the GNB is edge-on, and comparing the GNB trace with the corresponding Kikuchi diffraction. Accordingly, the upper and lower parts of GNB-I (which are the dominant segments of GNB-I) in Fig. 3c, is found to lie on the crystallographic plane (0.799 0.369 0.474), which is close to (although not ideally aligned with) the nearest slip plane, (111). The deviation between the GNB-I plane and (111) is 18°. Analogously, the crystallographic plane of GNB-II was determined as (0.461 0.633 -0.621), which is close to (11 $\bar{1}$) with a deviation of 8°.

3.2 Determination of Burgers vectors. The **g** vectors and their zone axes used for analysis of the two GNBs in this study are listed in Table 1. For each **g** vector, dislocations with a **b** vector that fulfills the condition that **g**·**b**=0 become invisible (Williams and Carter 1996). Assuming that all dislocations have **b** vectors of the ½<011> type, appropriate **g** vectors were chosen such that dislocations with different **b** vectors can be distinguished from each other according to their visibilities. Note that for many **b** vectors shown in Table 1, the associated dislocations are expected to be out of contrast at two **g** vectors; in such cases, the **b** of the dislocations can be unambiguously determined to be the one that is parallel to the cross product of the two **g** vectors, and **b** vectors of other types can be positively ruled out. It should be pointed out that in the present work, all the dislocations that were invisible at two **g** vectors are found to have **b** vectors of ½<011> type, which partly verifies the assumption of **b** vectors of the ½<011> type; **b** vectors of other types were not identified.

Table 1. Diffraction vectors chosen for Burgers vector analysis.

GNB-I									GNB-II								
Zone axis	**g**	**g**·**b** for different **b**s							Zone axis	**g**	**g**·**b** for different **b**s						
		b1	**b2**	**b3**	**b4**	**b5**	**b6**				**b1**	**b2**	**b3**	**b4**	**b5**	**b6**	
		10$\bar{1}$	01$\bar{1}$	1$\bar{1}$0	101	011	110	/2			10$\bar{1}$	01$\bar{1}$	1$\bar{1}$0	101	011	110	/2
$\bar{1}\,\bar{1}\,\bar{2}$	2$\bar{2}$0	1	-1	2	1	-1	0		11$\bar{2}$	2$\bar{2}$0	1	-1	2	1	-1	0	
	11$\bar{1}$	1	1	0	0	0	1			111	0	0	0	1	1	1	
	1$\bar{3}$1	0	-2	2	1	-1	-1			3$\bar{1}$1	1	-1	2	2	0	1	
	$\bar{3}$11	-2	0	-2	-1	1	-1			1$\bar{3}\,\bar{1}$	1	-1	2	0	-2	-1	
00$\bar{1}$	200	1	0	1	1	0	1		00$\bar{1}$	200	1	0	1	1	0	1	
	020	0	1	-1	0	1	1			020	0	1	-1	0	1	1	

Figure 4 shows the dislocation contents of GNB-I. The dislocation configuration is predominantly characterized by a hexagonal network while some rectangular networks can be found locally (Fig. 4d and e). Four prominent sets of dislocations, whose **b** vectors are **b1**, **b2**, **b3** and **b4** were identified (Fig. 4f). The **b** vectors were fully determined using the 6 **g** vectors listed in Table 1. Figure 4a-c show typical weak beam images using **g** vectors of [11 $\bar{1}$], [1 $\bar{3}$ 1] and [$\bar{3}$ 11], respectively. The **b1** dislocations (dislocations with **b** vectors of **b1**) are visible in both Fig. 4a and c, but invisible in Fig. 4b;

the **b2** dislocations are clearly revealed in Fig. 4a and b, while they disappear in Fig. 4c; both the **b3** and **b4** dislocations are out of contrast in Fig. 4a, but come in contrast in Fig. 4b and c. The **b1**, **b2** and **b3** dislocations compose the general hexagonal network, whereas the **b4** dislocations often crisscross the **b1** dislocations, forming local rectangular grids. Most of the dislocation lines appear rather straight, and dislocations from the same set are roughly parallel to each other. Besides the 4 sets of dislocations mentioned above, some dislocations with **b6** are also observed, whose amount is minor compared with that of the prominent dislocations.

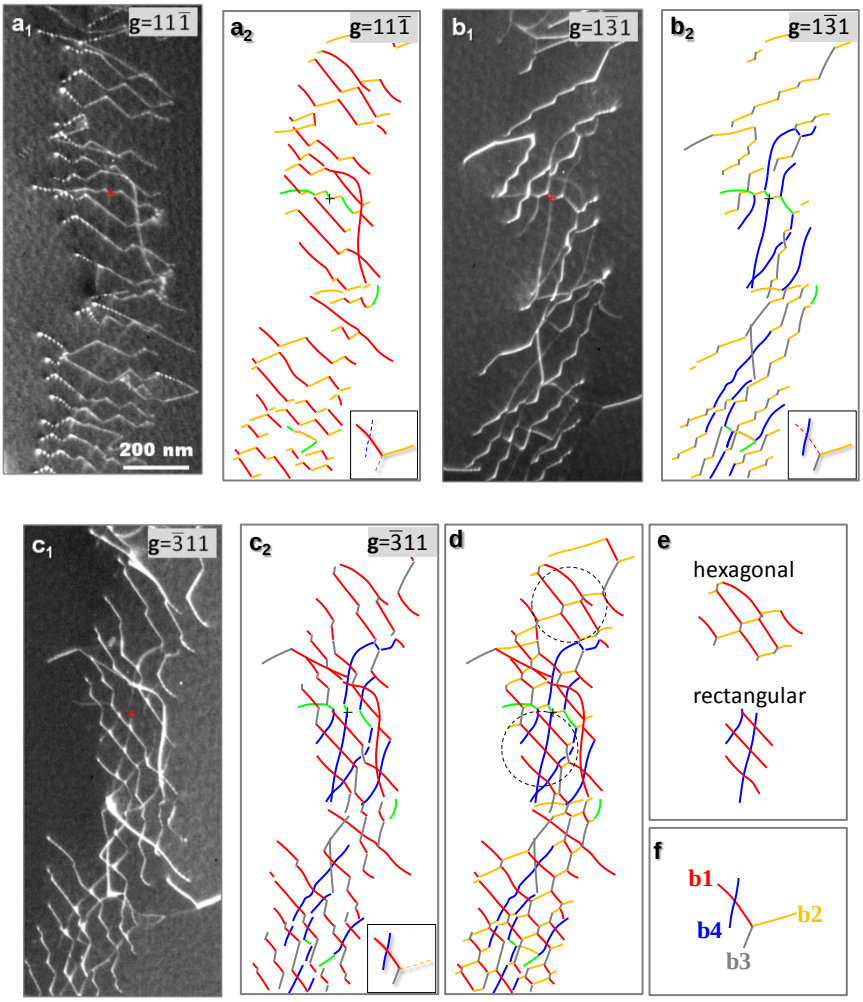

Fig. 4. Dislocation contents of GNB-I. (a_1,b_1,c_1) Weak-beam images using **g**=[11$\bar{1}$], **g**=[1$\bar{3}$1] and **g**=[$\bar{3}$11], respectively. (a_2,b_2,c_2) Schematic illustrations of (a_1), (b_1) and (c_1), respectively. The insets in the lower right corner indicate the dislocation visibilities, where solid lines represent visible dislocations and dashed lines represent invisible ones. (d) Illustration of all identified dislocations. (e) Two characteristic dislocation configurations extracted from the circled regions in (d). (f) Elemental dislocations of (d).

The dislocation contents of GNB-II are shown in Fig. 5. Four prominent sets of dislocations, with **b** vectors of **b2**, **b4**, **b5** and **b6** were identified (Fig. 5d and e). Figure 5a-c show typical weak-beam

images of GNB-II using **g** vectors of $[2\bar{2}0]$, [111] and $[3\bar{1}1]$, respectively. The **b2** dislocations are visible in Fig. 5a and c, but invisible in Fig. 5b; the **b4** dislocations are visible in all three images; the **b5** dislocations are visible in Fig. 5a and b, but invisible in Fig. 5c; the **b6** dislocations are invisible in Fig. 5a, but visible in Fig. 5b and c. The **b2**, **b4** and **b6** dislocations compose a hexagonal network, whereas the **b5** dislocations often crisscross the **b2** dislocations and form rectangular grids. Some **b1** dislocations and a few **b3** dislocations are also seen in GNB-II, but their number is much smaller compared with the dominant dislocations.

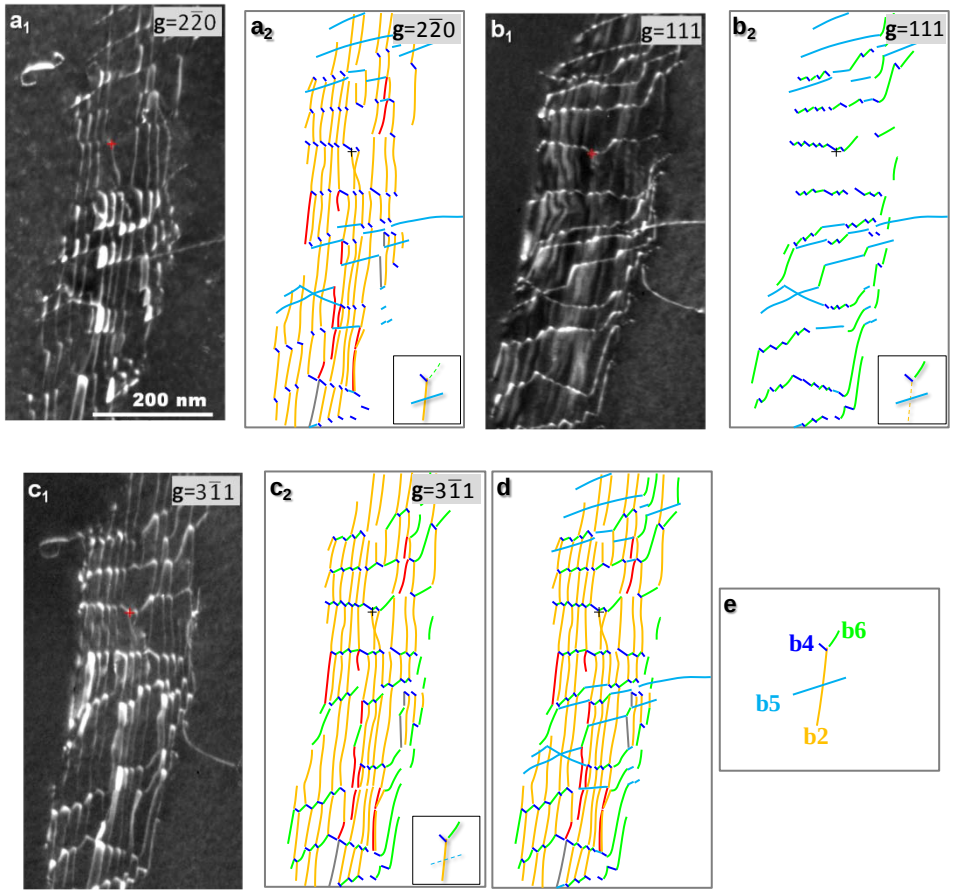

Fig. 5. Dislocation contents of GNB-II. (a_1,b_1,c_1) Weak-beam images using **g**=$[2\bar{2}0]$, **g**=[111] and **g**=$[3\bar{1}1]$, respectively. (a_2,b_2,c_2) Schematic illustrations of (a_1), (b_1) and (c_1), respectively. The insets indicate the dislocation visibilities, where solid lines represent visible dislocations and dotted lines represent invisible ones. (d) Illustration of all identified dislocations. (e) Elemental dislocations of (d).

3.3 Determination of dislocation line directions. Determination of dislocation line directions for GNB-I is shown in Fig. 6. Practically, only dislocations that lie on the dominant segments of GNB-I (those shown in Fig. 6a) were taken into account. One common plane that contains all the dislocations shown in Fig. 6a is the boundary plane of GNB-I, which has been determined to be (0.799 0.369 0.474) in Section 3.1. Therefore, to determine the line direction of a certain dislocation, only a second crystallographic plane that contains the dislocation is needed, which can be obtained from the trace

direction of the dislocation in Fig. 6a. Each dislocation in Fig. 6a was then fitted with linear segments (Fig. 6b). The statistical distribution of the trace directions was then obtained for each set of dislocations (Fig. 6c).

Clearly the trace directions for each set of dislocations have a narrow distribution, with the standard deviation being normally less than 10°. To simplify the calculation, for each set of dislocations, their average trace direction obtained based on Fig.6a (which is a projection image) is used to determine a second plane that "on average" contains the whole set of dislocations. Thus the average line directions of the **b1**, **b2**, **b3** and **b4** dislocations were determined to be [0.555 -0.153 -0.817], [0.034 0.760 -0.649], [0.533 -0.800 -0.276] and [0.483 -0.865 -0.140], respectively. The line directions for the **b2**, **b4**, **b5** and **b6** dislocations in GNB-II were determined as [0.827 -0.560 0.044], [0.637 0.252 0.729], [0.032 0.688 0.725] and [0.552 -0.753 -0.358], respectively.

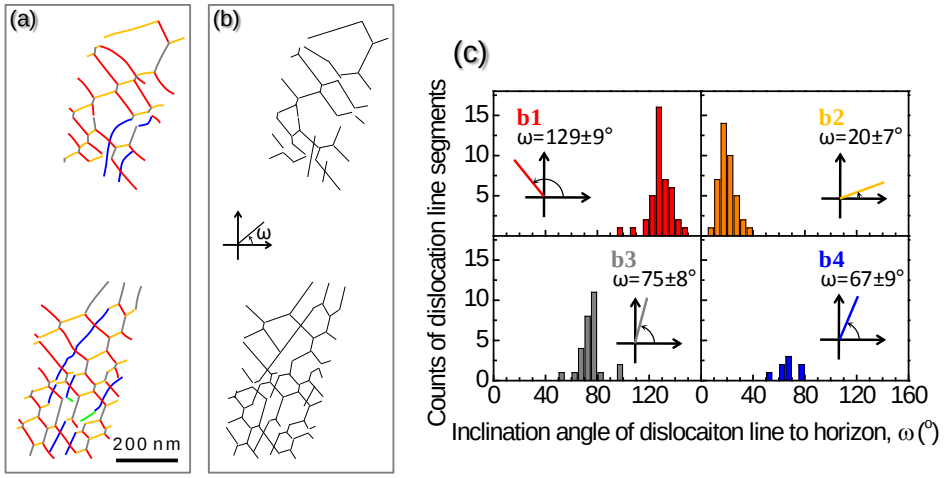

Fig. 6. Acquisition of dislocation trace directions on a projection image for the dominant segment of GNB-I. (a) Dislocation traces from weak-beam images in Fig. 4. (b) Linear segmentation of the dislocation traces in (a). (c) Statistic distribution of trace directions for each of the 4 sets of dislocations shown in (a), in terms of the inclination angle to image horizon, ω, as measured from (b).

The measured line directions of the GNB dislocations exhibit the characteristics of glide dislocations that remain on the slip planes predicted active. As for **b1** or **b2** dislocations on GNB-I, as well as for **b4** or **b5** dislocations on GNB-II, where the slip plane predicted active of the dislocations is approximately parallel to the GNB plane, the dislocations have primarily a screw character. On the other hand, as for **b2** dislocations on GNB-II, or **b4** dislocations on GNB-I, where the slip plane predicted active inclines steeply to the GNB plane, the dislocations approximately coincide with the line of intersection between the predicted slip plane and the GNB, and thus have a large edge component in their character.

4. DISCUSSION AND CONCLUDING REMARKS

Most of the dislocations observed in the two GNBs have Burgers vectors corresponding to the expected active slip directions, i.e. **b1**, **b2**, **b4** and **b5**. This is in good agreement with the fact that the type of dislocation boundaries, in particular their crystallographic alignment, depends on the grain orientation

and further correlates with the expected slip. Nevertheless, dislocations with the two other Burgers vectors relevant for fcc metals are also well-represented, namely **b3** and **b6**. Their occurrence may be attributed to reactions between the dislocations gliding on these four slip systems or activation of more than the initially expected four slip systems.It is energetically favourable for two dislocations with Burgers vectors b_a and b_b to react and form a dislocation with b_c if $|b_a|^2+|b_b|^2>|b_c|^2$ (Hirth and Lothe 1968). Reaction between **b1** and **b2** resulting in **b3** dislocations in GNB-I is energetically favoured, and so is reaction between **b2** and **b4** giving rise to **b6** in GNB-II. Two main types of dislocation networks are observed in the GNBs. One is in GNB-I, which mainly contains 3 sets of dislocations in a hexagonal network all having Burgers vectors (**b1**, **b2** and **b3**) in the slip plane with which the boundary aligned. The other is in GNB-II, which mainly contains 4 sets of dislocations and involves Burgers vectors (**b2**, **b4**, and **b5**) coming from both of the slip planes expected active. The reaction product **b6** dislocations in GNB-II do not lie in a possible slip plane and is a sessile Lomer lock (Hirth and Lothe 1968).

In the analysis of dislocation configurations in GNBs Frank equation is applied (Frank 1950; Frank 1951). Dislocation arrangements that fulfil this equation are low-energy-dislocation-structures (LEDS) (Kuhlmann-Wilsdorf 1989) free of long-range stresses. Using the Frank equation and assuming that all boundary dislocations come from one of the four slip systems predicted active, and that the dislocations only move by glide in their slip plane, configurations similar to the two types of dislocation networks observed here can be predicted for a GNB lying exactly on the (111) slip plane (Winther 2012). The measured misorientation angles across the two GNBs are within the usually assumed bounds of b/D and b/2D with D being the measured mean spacing of all dislocations. The GNBs observed here are therefore most likely LEDS. McCabe et al. (2004) characterized the dislocations in a slip-plane-aligned GNB in a rolled copper grain also expected to slip on two sets of coplanar systems but not symmetrically as in the 45°ND-rotated Cube. They also found that the boundary dislocations came from the active systems and observed Lomer locks. The detailed dislocation configuration in the boundary was found to fulfil the Frank equation (Frank 1951) for boundaries free of long-range stresses but this arrangement, however, was a regular square grid of dislocation lines, which differs substantially from the configurations observed here. Wei et al. (2011) found that the dislocation configurations in 11 similarly oriented cell boundaries investigated in rolled aluminium grains of near Cube orientation all were identical square grids, for which the Frank equation was also fulfilled.

It has been recently shown that three types of dislocation boundaries can form in deformed metals, including IDBs, slip-plane-aligned GNBs, and non-slip-plane-aligned GNBs (Huang and Winther 2007; Winther and Huang 2007). A complete data set of dislocation contents on all three types of boundaries is then necessary for a thorough understanding of the formation and evolution of deformation induced dislocation boundaries. Characterization of non-slip-plane-aligned GNBs in cold rolled pure Al samples near {112}<111> orientation are therefore in progress. By combining these observations a deeper insight can be obtained as to how dislocation boundaries form and evolve during plastic deformation to underpin analytical and numerical models which may also include strengthening.

ACKNOWLEDGEMENTS

The authors acknowledge support from the Danish National Research Foundation and the National Natural Science Foundation of China (Grant No. 50911130230) for the Danish-Chinese Center for Nanometals. Discussions with Drs. N. Hansen and A. Godfrey are gratefully acknowledged.

REFERENCES

Bay, B., Hansen, N., Hughes, D., Kuhlmann-Wilsdorf, D. (1992). Overview No-96 - Evolution of Fcc Deformation Structures in Polyslip. Acta Metallurgica Et Materialia, 40(2), 205-219.

Frank, F. (1950). The resultant content of dislocations in an arbitrary intercrystalline boundary. Symposium on Plastic Deformation of Crystalline Solids. Mellon Institute of Industrial Research. Pittsburgh, 150-154.

Frank, F. (1951). Crystal Dislocations - Elementary Concepts and Definitions. Philosophical Magazine, 42(331), 809-819.

Hansen, N. & Huang, X. (1998). Microstructure and flow stress of polycrystals and single crystals. Acta Materialia, 46(5), 1827-1836.

Hirth, J. P. & Lothe, J. (1968). Theory of dislocations. New York, St. Louis, San Francisco, Toronto, London, Sydney: McGraw-Hill.

Huang, X. & Liu, Q. (1998). Determination of crystallographic and macroscopic orientation of planar structures in TEM. Ultramicroscopy, 74(3), 123-130.

Huang, X. & Winther, G. (2007). Dislocation structures. Part I. Grain orientation dependence. Philosophical Magazine, 87(33), 5189-5214.

Hughes, D., Khan, S., Godfrey, A., Zbib, H. (2001). Internal structures of deformation induced planar dislocation boundaries RID G-4458-2010. Materials Science and Engineering A-Structural Materials Properties Microstructure and Processing, 309, 220-226.

Kuhlmann-Wilsdorf, D. (1989). Theory of Plastic-Deformation - Properties of Low-Energy Dislocation-Structures. Materials Science and Engineering A-Structural Materials Properties Microstructure and Processing, 113, 1-41.

Li, Z., Godfrey, A., Liu, Q. (2004). Evolution of microstructure and local crystallographic orientations in rolled Al-1%Mn single crystals of {001} orientation. Acta Materialia, 52(1), 149-160.

Lin, F. X., Godfrey, A., Winther, G. (2009). Grain orientation dependence of extended planar dislocation boundaries in rolled aluminium. Scripta Materialia, 61(3), 237-240.

McCabe, R., Misra, A., Mitchell, T. (2004). Experimentally determined content of a geometrically necessary dislocation boundary in copper. Acta Materialia, 52(3), 705-714.

Wei, Y. L., Godfrey, A., Liu, W., Liu, Q., Huang, X., Hansen, N., Winther, G. (2011). Dislocations, boundaries and slip systems in cube grains of rolled aluminium. Scripta Materialia, 65(4), 355-358.

Wert, J. A., Huang, X., Winther, G., Pantleon, W., Poulsen, H. F. (2007). Revealing deformation microstructures. Materials Today, 10(9), 24-32.

Williams, D. B. & Carter, C. B. (1996). Transmission Electron Microscopy. New York: Plenum Press.

Winther, G. (2005). Effect of grain orientation dependent microstructures on flow stress anisotropy modelling. Scripta Materialia, 52(10), 995-1000.

Winther, G. & Huang, X. (2007). Dislocation structures. Part II. Slip system dependence. Philosophical Magazine, 87(33), 5215-5235.

Winther, G. (2012). Theoretical analysis of slip-plane-aligned geometrically necessary dislocation boundaries originating from two sets of coplanar slip systems.

Winther, G. (2008). Slip systems extracted from lattice rotations and dislocation structures. Acta Materialia, 56(9), 1919-1932.